

A&A manuscript no.
(will be inserted by hand later)

Your thesaurus codes are:
10(10.01.1;10.05.1;10.06.1;10.06.2)

Two-component model for the chemical evolution of the Galactic disk

R.X. Chang, J.L. Hou, C.G. Shu and C.Q. Fu

Shanghai Astronomical Observatory, Chinese Academy of Sciences, Shanghai, 200030, China

Abstract. In the present paper, we introduce a two-component model of the Galactic disk to investigate its chemical evolution. The formation of the thick and thin disks occur in two main accretion episodes with both infall rates to be Gaussian. Both the pre-thin and post-thin scenarios for the formation of the Galactic disk are considered. The best-fitting is obtained through χ^2 -test between the models and the new observed metallicity distribution function of G dwarfs in the solar neighbourhood (Hou et al 1998). Our results show that post-thin disk scenario for the formation of the Galactic disk should be preferred. Still, other comparison between model predictions and observations are given.

Key words: Galaxy: abundance - Galaxy: evolution; formation - Galaxy: fundamental parameters

1. Introduction

Since the existence of the thick disk of our Galaxy was confirmed by Gilmore & Reid (1983) more than ten years ago, it has been generally accepted that a complete description of the thick disk, such as its scale length, scale height, density normalization, metallicity and kinematical properties, is a necessary step towards understanding the Galaxy formation, halo collapse, disk dynamical and chemical evolution. Unfortunately, the characteristics of this population remain controversial, especially for its density profile. Several attempts have been made to deduce this parameter by remote star counts and field star survey (Buser & Kaeser 1985, Gilmore, Reid & Hewett 1985, Reid & Majewski 1993, Buser, Rong & Karaali 1998). But the results are still quite uncertain. This is partly due to the lack of complete sample of thick disk stars since its members cannot be easily recognized from that of the thin disk and/or the halo in most observable

distributions. Moreover, the determination of thick disk characteristics requires large star samples in various directions well distributed in both the longitude and latitude (Robin et al. 1996), which cannot be obtained easily at the present time.

Recently, the study of chemical evolution of the Galactic disk has been proven to be a powerful tool to explore the formation and evolution of our Galaxy. Numerous models have been detailedly put forward (Matteucci & Francois 1989, Ferrini et al. 1994, Giovagnoli & Tosi 1995, Prantzos & Aubert 1995, Timmes et al. 1995, Carig 1996, Pilyugin & Edmunds 1996a, Chiappini, Matteucci & Gratton 1997, Allen et al. 1998, Thon & Meusinger 1998, Prantzos & Silk 1998). Among them, Chiappini, Matteucci & Gratton (1997 hereafter CMG97) were the first to take into account the effect of thick disk. They assumed that there are two main accretion episodes. The first is responsible for the formation of the thick disk, and the second, delayed relative to the first, forms the thin disk. The predictions of their best-fitting model are in good agreement not only with the observed metallicity distribution, but with the observed number of very low metallicity stars (Rocha-Pinto & Maciel 1996, hereafter RM96). This enlightens us to do more detailed analyze of the disk evolution based on the new chemical constraints.

In the present paper, the two-component model for the Galactic disk evolution (such as CMG97) is adopted, in which the local surface density of the thick disk at the present time is chose to be one of the free parameters. The infall rate is assumed to be in a Gaussian form instead of an exponentially decreasing one. The quantitative comparison between model predictions and the observations, i.e., the new G-dwarf metallicity distribution obtained by Hou et al (1998), is used for the χ^2 -test of the best-fitting model.

The outlines are as follows. In section 2, we present brief description of observational constraints up to now, of which the most important is the G-dwarf metallicity distribution. Section 3 is the model and its main ingredients. In section 4, we present best-fittings of four different models, which are closed-box, one-component, pre-thin and post-thin models respectively, to the observations. Discussions of the models are also included in section 4. Our conclusions are shown in the last section.

2. Observational constraints

A successful model of the chemical evolution of the galactic disk should reproduce the main observational features of both the solar neighborhood and whole disk. Our set of constraints includes:

- (1) G-dwarf metallicity distribution in the solar neighbourhood (Hou et al 1998);
- (2) radial abundance gradients at present time;
- (3) age-metallicity relation (AMR);

- (4) the correlation between [O/Fe] and [Fe/H];
- (5) radial profiles for the gas surface density; and
- (6) the variations of Star Formation Rate (SFR) across the disk.

The first one is selected as the observational constraint to quantitatively estimate the best-fitting model in this paper, since G dwarfs cover the whole life of the Galactic disk and its metallicity distribution can reflect the local chemical enrichment history. The others are used for the comparisons between the best-fit model predictions and observations.

2.1. *G-dwarf metallicity distribution*

The metallicity distribution of G dwarfs in the solar neighborhood is one of the most important constraints on the chemical evolution of the Galactic disk. Since G dwarfs have lifetimes comparable to the estimated age of the Galaxy, they represent a sample which has never been depleted by stellar evolution, accumulating since the first episodes of low-mass star formation. Therefore, a complete sample of these stars in the solar neighborhood carries memory of the local star formation and chemical enrichment history.

Pagel & Patchett (1975) derived a cumulative G-dwarf metallicity distribution, based on a volume-limited sample of 132 G dwarfs within about 25 pc of the Sun. Pagel (1989) revised previous data of Pagel & Patchett (1975) by means of a new calibration between the ultraviolet excess δ (U-B) and [Fe/H]. Later, Rana (1991) and Sommer-Larsen (1991) independently revised the distribution of Pagel (1989), taking into account the dynamical heating effect on the observed distribution. RM96 derived a G-dwarf metallicity distribution in the solar neighborhood, using *uvby* photometry and up-to-date parallaxes. RM96 introduced a chemical criterion, according to which all stars have $[\text{Fe}/\text{H}] < -1.2$ are considered to be halo members and excluded from the final sample. The distribution of RM96 comprises 287 G dwarfs within 25 pc from the Sun and differs from the classic one by having a prominent single peak around $[\text{Fe}/\text{H}] = -0.2$ (see RM96 for details).

Recently, Hou et al (1998) collected a new, enlarged sample of G dwarfs within 25pc from the Sun. The stars are selected from the third Catalogue of Nearby Stars (Gliese & Jahreiss 1991). The *uvby* data are taken from the catalogues of Olsen (1993) and Hauck & Mermilliod (1990). No chemical criterion was introduced in Hou et al (1998) since observational evidences showed that, in the metallicity interval $-1.5 < [\text{Fe}/\text{H}] < -1.0$, the fraction of thick disk stars in the solar neighbourhood appears to be as high as 60% (Nissen & Schuster 1997). This is one of the main differences between the distribution of Hou et al (1998) and that of RM96. The final sample contains 382 G dwarfs with photometric data. The adopted metallicity calibration and kinetic correction is the same

Table 1. The obtained G-dwarf metallicity distribution in the solar neighbourhood taken from Hou et al (1998)

[Fe/H]	ΔN_0	f	$\delta(\Delta N_0)$	$\frac{\Delta N_0/f+\delta(\Delta N_0)}{N}$
-1.5 ~ -1.4	1	0.23	-0.163	0.0091508
-1.4 ~ -1.3	2	0.23	-1.276	0.0110225
-1.3 ~ -1.2	2	0.23	-0.422	0.0110225
-1.2 ~ -1.1	0	0.23	-0.571	0.0110225
-1.1 ~ -1.0	1	0.23	-0.670	0.0177367
-1.0 ~ -0.9	0	0.23	-0.646	0.0177367
-0.9 ~ -0.8	5	0.23	-0.437	0.0177367
-0.8 ~ -0.7	8	0.36	-0.030	0.0485269
-0.7 ~ -0.6	12	0.53	0.513	0.0506311
-0.6 ~ -0.5	22	0.79	1.055	0.0632013
-0.5 ~ -0.4	22	0.85	1.430	0.0597229
-0.4 ~ -0.3	44	0.98	1.511	0.1014807
-0.3 ~ -0.2	56	0.99	1.270	0.1264671
-0.2 ~ -0.1	62	1.00	0.790	0.1373006
-0.1 ~ 0.0	58	1.00	0.217	0.1273009
0.0 ~ 0.1	47	1.00	-0.260	0.1022046
0.1 ~ 0.2	29	1.00	-0.569	0.0621690
0.2 ~ 0.3	10	1.00	-0.678	0.0203841
0.3 ~ 0.4	3	1.00	-0.630	0.0051824

as that of RM96. Following Pagel (1989) and RM96, Hou et al (1998) have also corrected the distribution for observational errors and cosmic scatter. The results of Hou et al (1998) are shown in Table 1, in which the sample is divided into 19 bins. The first column of Table 1 is the metallicity range in each bin. The raw distribution (ΔN_0) are presented in column 2. The third is the weight factor f_i for the scale height correction according to Sommer-Larson (1991). The fourth presences $\delta(\Delta N_0)_i$, the correction factors for the observational errors and cosmic scatter. The obtained relative distribution is given in the last column, where $N = \sum_{i=1}^{19} [\frac{(\Delta N_0)_i}{f_i} + \delta(\Delta N_0)_i]$ is the total number of G dwarfs after correction. In the last column, the second to fourth bins are grouped to yield a mean value for the distribution, which is similar with the method used in RM96. This procedure is also used for the fifth to seventh bins. Table 1 shows that the resulted distribution of Hou et al (1998) differs from that of RM96 by having a larger width and smaller amplitude of the single peak. Moreover, the metal-poor tail of the new distribution (Hou et al 1998) extends to [Fe/H]=-1.5.

2.2. Abundance gradients

Furthermore, radial metallicity variations of the interstellar medium (ISM) can constrain models of Galaxy formation and chemical evolution. From extensive studies of optical emission lines in HII regions, Shaver et al. (1983) derived an oxygen abundance gradient of the order of -0.07 dex/kpc. Afflerbach et al. (1996) have indirectly deduced a similar result by measuring electron temperature variations in a set of ultra-compact HII regions. A relatively flatter gradient has been obtained by Vilchez & Esteban (1996) for the outer Galaxy, using spectroscopic observations of a sample of HII regions towards the Galactic anti-center.

The recent radial profile of oxygen in the Galaxy can also be traced by observations of B-type stars, with main sequence ages less than 1.0 Gyr. A series of medium- to high-resolution spectroscopic observations of early B-type main-sequence objects have been published (Smartt et al. 1997 and references therein). Using this homogeneous sample, Smartt et al. (1997) derived an oxygen abundance gradient of -0.07 ± 0.01 dex/kpc between Galactocentric distance of $6 \text{ kpc} \leq r \leq 18 \text{ kpc}$, which is in good agreement with nebular studies. Gummersbach et al. (1998) determines the stellar parameters and abundances of several elements for 16 early B main-sequence stars in Galactocentric distance $5.0 \text{ kpc} \leq r \leq 14.0 \text{ kpc}$ by reanalyzing and extending the observations of Kaufer et al. (1994). An oxygen abundance gradient -0.07 ± 0.01 dex/kpc is derived, typical for normal spiral galaxies of similar Hubble type.

2.3. Others

Just as mentioned above, other chemical constraints should be taken into account at the same time, such as the age-metallicity relation, the correlation between $[\text{O}/\text{Fe}]$ and $[\text{Fe}/\text{H}]$ for field stars as well as the radial profiles of gas surface density and SFR at the present time for the whole disk.

Twarog (1980) obtained the first AMR for the local disk stars, with the stellar ages from the theoretical isochrones. The same sample has been reanalyzed by Carlberg et al. (1985) with different results, due to the revision of the isochrones as well as the calibration of abundances. A more accurate AMR was obtained by Edvardsson et al. (1993). They have derived abundances of 13 different elements, such as O, Fe, Si, Ba etc., as well as individual photometric ages, for 189 nearby field F and G dwarfs. Their abundance analysis was made with theoretical LTE model atmospheres, based on the extensive high resolution, high S/N, spectroscopic observations of carefully selected field stars. The resulted AMR of Edvardsson et al. (1993) was used at the present study. However, this AMR does not constitute a tight constraint of the chemical model, since there is a considerable scatter. Moreover, the results of the survey of Edvardsson et

al. (1993) concerning O vs. Fe relationships for field stars are used in this study. As for metal-poor stars, the correlation between [O/Fe] and [Fe/H] are taken from Barbuy (1988).

The radial Galactic profiles of atomic and molecular hydrogen are discussed in Lacey & Fall (1985). An updated discussion is given in Dame (1993). Inside the solar circle, the molecular and atomic gas are found in roughly equal amounts. However, the surface density of atomic hydrogen, which seems to be constant from 4kpc to 15kpc , dominates the gas profiles outside the solar circle. The radial distribution of the sum of atomic and molecular hydrogen given in Dame (1993) is adopted in this paper.

The radial distribution of the present SFR in the Galaxy are taken from Gusten & Merger (1983), Lyne et al (1983) and Guibert et al (1978). Data are based on several tracers of star formation: Lyman continuum photons from HII regions, pulsars and supernova remnants. It is normalized to the present SFR in the solar neighbourhood (as in Lacey & Fall 1985) since the absolute values depend on poorly known conversion factors.

3. The model

It is assumed that the Galactic disk is sheet-like, which originates and grows only from the infall of primordial gas. The disk is considered as a system of independent rings with 1kpc wide for each. No radial inflows or outflows are considered and the center of each ring locates at its median Galactocentric radius. The ring centered at Galactocentric distance $r_\odot = 8.5\text{ kpc}$ is labeled as the solar neighbourhood. The age of the disk is adopted to be 13.0Gyr (Rana 1991).

3.1. Basic equations and nucleosynthesis

The instantaneous-recycling approximation (IRA) is relaxed, but instantaneous mixing of the gas with the stellar ejecta is assumed, i.e., the gas is characterized by a unique composition at each epoch of time. We solve numerically the classical set of equations of Galactic chemical evolution (Tinsley 1980, Pagel 1997) as

$$\frac{d\Sigma_{tot}(r, t)}{dt} = f(r, t), \quad (1)$$

$$\frac{d\Sigma_{gas}(r, t)}{dt} = -\psi(r, t) + \int_{m_t}^{100} (m - m_r) \psi(r, t - \tau_m) \phi(m) dm + f(r, t), \quad (2)$$

$$\frac{d[Z_i(r, t)\Sigma_{gas}(r, t)]}{dt} = -Z_i(r, t)\psi(r, t) + \int_{m_t}^{100} m y_{i,m} \psi(r, t - \tau_m) \phi(m) dm + Z_{i,f} f(r, t) \quad (3)$$

where $\Sigma_{tot}(r, t)$ and $\Sigma_{gas}(r, t)$ are the total and gas surface density respectively in the ring centered at Galactocentric distance r at evolution time t ; $f(r, t)$ is often called the infall or accretion rate; $\psi(r, t)$ is the star formation rate (SFR) and $\phi(m)$ is the initial mass function (IMF); m_r and τ_m are the remnant mass and the lifetime of a star of initial

mass m , respectively, and m_t is the corresponding initial mass of a star whose main-sequence lifetime τ_m equates to evolution time t (the turnoff mass). Here the mass range of IMF is taken from $0.1M_\odot$ to $100M_\odot$. The mass of element i in the gas evolves via star formation (putting metals from the ISM into stars), ejection, and gas inflows, according to equation (3), where $y_{i,m}$ is the stellar yield of element i , i.e., the mass fraction of a star of initial mass m that is converted to element i and ejected, and $Z_{i,f}$ is the mass abundance of element i in the infalling gas, which is assumed to be primordial in this study: $Z_{O,f} = Z_{Fe,f} = 0$. It should be emphasized that the second terms in the right hand of equations (2) and (3) also include the contribution of Type Ia supernovas (Type Ia SNe), which is detailedly presented in Matteucci & Greggio (1986). The constant A in equation (9) of Matteucci & Greggio (1986) describes the fraction of systems with total mass in appropriate range, which eventually succeed in giving rise to a Type Ia SN event, and in this study, it is fixed by requiring to present best-fit to the metal-rich tail of the G-dwarf metallicity distribution in the solar neighbourhood.

It is also assumed that every star ejects its envelope just after leaving the main sequence. The adopted relation between main-sequence lifetimes τ_m (in units of Gyr) and stellar initial mass m (in units of M_\odot) is (Larson 1974):

$$\log m = 1.983 - 1.054\sqrt{(\log \tau_m + 2.52)}. \quad (4)$$

For the sake of simplicity, we assume that, except for Type Ia SNe, any star evolves as a single star even if it is the member of a binary system. All massive stars ($m > 9M_\odot$) explode as type II supernovas (Type II SNe), leaving behind a neutron star of mass $m_R = 0.5M_\odot$ (Prantzos & Silk 1998). The final stage of the intermediate /low mass stars ($M \leq 9M_\odot$) is white dwarfs, and the final-initial mass relation is taken from Weidemann(1984). Type Ia SNe are thought to originate from carbon deflagration in C-O white dwarfs in binary systems. The method included the contribution of Type Ia SNe is the same as Matteucci & Greggio (1986).

In this paper, we only consider the evolution of iron and oxygen. The oxygen and iron production for Type II SNe and Type Ia SNe are taken from Woosley & Weaver (1995) and Woosley (1997), respectively. Recently, using the evolutionary tracks of Geneva group up to the early asymptotic giant branch (AGB) in combination with a synthetic thermal-pulsing AGB model, van den Hock & Groenewegen (1997) calculated in detail the chemical evolution and yields of six elements up to the end of AGB. Their results showed that the low-mass stars ($m < 3M_\odot$) produce small amounts of oxygen, yet the intermediate mass stars ($3M_\odot \leq m \leq 8M_\odot$) destroy the initial oxygen through Hot Bottom Burning (HBB). Therefore, it is reasonable in this paper to neglect the oxygen production by intermediate/low mass stars compared with that of massive stars.

3.2. The infall rate

Currently popular models of the galaxy formation are semi-analytic models within the framework of the hierarchical structure formation paradigm (White & Rees 1978, White & Frenck 1991, Wechsler et al 1998, Mo et al 1998), which allow one to model the astrophysical processes involved in galaxy formation in a simplified but physical way (Kauffmann et al 1993, Somerville & Primack 1998, Kauffmann et al 1998, Primack et al 1998). These models are in good agreement with a broad range of local galaxy observations, including the correlation between luminosity and circular velocity for spirals (the Tully-Fisher relation), the B-band luminosity function, cold gas contents, metallicities, and colors. These models postulate that the formation of galaxy is mainly regulated by gas cooling, dissipation, star formation, and supernova feedback. However, for the purpose of simplicity, Galactic chemical evolution models assume that the integral effect of these processes can be represented by that of an infall rate, which is a function of evolution time and Galactocentric distance. The form of the infall rate is adjusted to satisfy the constraint of G-dwarf metallicity distribution in the solar neighbourhood. Although an exponentially decreasing infall rate is widely used, we adopt here a Gaussian form for the infall rate. The physical motivation for such a choice is that because of its small initial surface density, the local disk initially accretes a small amount of the surrounding gas; as the disk mass and gravitational potential build up, the accretion rate gradually increases, but starts decreasing when the gas reservoir is depleted (Prantzos & Silk 1998).

Numerous models for the formation of thick disk have been put forward since the confirmation of its existence by Gilmore & Reid (1983) (see Majewski 1993 for details). The models fall into either "top-down" scenarios (the pre-thin model), where the formation of the thick disk precedes that of the thin disk, or the "bottom-up" scenarios (the post-thin model), where the thick disk is the result of some action on or by the thin disk. In the pre-thin disk model, the formation of the thick disk is a transitional phase during the general contraction of the Galaxy. This model views the thick disk as a dissipative, rotational-supported structure, and the halo as non-dissipative and supported by the kinetic pressure provided by large, anisotropic velocity dispersions. The post-thin model resorts to formation of the thick disk after the gas has completely collapsed into a thin disk. Possible physical processes are: (1) Secular kinematic diffusion of thin disk stars (Norris 1987); (2) Violent thin disk heating by the accretion of a satellite galaxy (Quinn et al 1993). The required events must not occur too late in the disk life time so that the gas can cool again and form stars in the thin disk; (3) Halo response to disk potential (Gilmore & Reid 1983). The post-thin model leaves two important observational signatures. First, the thick disk is a separate population distinct from the thin disk and the

halo. Second, no gradient can be generated in the thick disk by the events, although a pre-existing gradient may survive the merger.

In this study, both the pre-thin and post-thin model for the formation of Galactic disk are considered. Following CMG97, we assume that there are two main infall episodes in both cases. The rate of mass accretion (in unit of $M_{\odot} pc^{-2} Gyr^{-1}$) in each ring could be expressed as

$$f(r, t) = \frac{A(r)}{\sqrt{2\pi}\sigma_t} e^{-(t-\tau_t)^2/2\sigma_t^2} + \frac{B(r)}{\sqrt{2\pi}\sigma_d} e^{-(t-\tau_d)^2/2\sigma_d^2}, \quad (5)$$

where τ_t and τ_d (in units of Gyr) are the maximum infall time of the thick and thin disk respectively, σ_t and σ_d (in units of Gyr) are the corresponding half-width. It is assumed that $\sigma_t \approx \tau_t$ and $\sigma_d \approx \tau_d$, i.e., the value of the half-width can just varies a little around that of the formation time-scale (Prantzos & Silk 1998).

For the pre-thin model, the first infall episode forms the thick disk, which originated from a fast dissipative collapse such as that suggested by Eggen, Lynden-Bell & Sandage (1962) (Sandage 1990, Majewski 1993, CMG97). The second infall episode, delayed to the first, forms the thin disk component, with a time-scale much longer than that of the thick disk. The infall rate $f(r, t)$ is normalized to the local disk density at present time, i.e., $\int_0^{t_g} f(r, t) dt = \Sigma_{tot}(r, t_g)$. Assuming the total masses of different rings in the disk at the present time are all exponentially decreased with the increase of Galactocentric distance for thin and thick disk with the same scale-length r_0 , the form of $A(r)$ and $B(r)$ in the pre-thin model can be written respectively as

$$A(r) = \frac{\Sigma_{thick}(r_{\odot}, t_g)}{\int_0^{t_g} \frac{e^{-(t-\tau_t)^2/2\sigma_t^2}}{\sqrt{2\pi}\sigma_t} dt} e^{-\frac{r-r_{\odot}}{r_0}} \quad (6)$$

$$B(r) = \begin{cases} 0 & \text{if } t < t_{max} \\ \frac{\Sigma_{tot}(r_{\odot}, t_g) - \Sigma_{thick}(r_{\odot}, t_g)}{\int_{t_{max}}^{t_g} \frac{e^{-(t-\tau_d)^2/2\sigma_d^2}}{\sqrt{2\pi}\sigma_d} dt} e^{-\frac{r-r_{\odot}}{r_0}} & \text{if } t_{max} \leq t \leq t_g \end{cases} \quad (7)$$

respectively, where t_g is the age of the Galactic disk, t_{max} represents the epoch of time at which the formation of the thin disk begins, $\Sigma_{tot}(r_{\odot}, t_g)$ is the present total surface density in the solar neighborhood, and $\Sigma_{thick}(r_{\odot}, t_g)$ is the local surface density of the thick disk at the present time, which is one of the free parameters in our model. We adopted $r_0 = 2.7$ kpc (Robin et al 1996, Kent 1992), and $\Sigma_{tot}(r_{\odot}, t_g) = 55.0 M_{\odot} pc^{-2}$ (Rana 1991, Sackett 1997) for Galactic disk. There are four free parameters in the pre-thin model, τ_t, τ_d, t_{max} and $\Sigma_{thick}(r_{\odot}, t_g)$.

Contrary to the pre-thin model, the post-thin model assumes the first infall episode forms thin disk. Then, the thick disk forms delayedly as a result of some actions on or by the thin disk. Using the same method described above, the form of $A(r)$ and $B(r)$ in

the post-thin model can be written as

$$A(r) = \begin{cases} 0 & \text{if } t < t_{max} \\ \frac{\Sigma_{thick}(r_{\odot}, t_g)}{\int_{t_{max}}^{t_g} \frac{e^{-(t-\tau_d)^2/2\sigma_d^2}}{\sqrt{2\pi}\sigma_d} dt} e^{-\frac{r-r_{\odot}}{r_0}} & \text{if } t_{max} \leq t \leq t_g, \end{cases} \quad (8)$$

$$B(r) = \frac{\Sigma_{tot}(r_{\odot}, t_g) - \Sigma_{thick}(r_{\odot}, t_g)}{\int_0^{t_g} \frac{e^{-(t-\tau_t)^2/2\sigma_t^2}}{\sqrt{2\pi}\sigma_t} dt} e^{-\frac{r-r_{\odot}}{r_0}}, \quad (9)$$

respectively, where each parameter has the same notation as Eq. (6) and (7) except t_{max} , which represents the epoch of time at which the thick disk begins to form. There are also four free parameters in the pre-thin model, τ_t , τ_d , t_{max} and $\Sigma_{thick}(r_{\odot}, t_g)$.

3.3. SFR and IMF

In the majority of chemical evolution models, star formation rate (SFR) is assumed to depend on some power of the gas surface density (Prantzos & Aubert 1995, Tosi 1996, CMG97). Based on gravitational instability, Wang & Silk (1994) developed a self-consistent model to derive the global star formation rate as a function of radius in galactic disks. The resulted star formation rate not only depends on the gas surface density, but also is proportional to the epicycle frequency κ . Since $\kappa \propto r^{-1}$, we adopt a similar star formation rate as that of Prantzos & Aubert (1995), which can be expressed as (in units of $M_{\odot}pc^{-2}Gyr^{-1}$) :

$$\psi(r, t) = \nu \Sigma_{gas}^n(r, t) / r \quad (10)$$

where $\Sigma_{gas}(r, t)$ and r are in units of $M_{\odot}pc^{-2}$ and kpc , respectively. The power law index $n = 1.4$ is adopted (Prantzos & Silk 1998), which is in some degree similar to that of Kennicutt (1998). The value of ν is derived from the condition of reproducing the present observed gas surface density in the solar neighborhood. We adopted $\Sigma_{gas}(r_{\odot}, t_g) = 10.0 M_{\odot}pc^{-2}$ (Scoville & Sanders 1987, Prantzos & Aubert 1995, Sackett 1997).

The adopted stellar initial mass function (IMF) is taken from Kroupa et al. (1993), in which the IMF is described by a three-slope power law, $\phi(m) \propto m^{-(1+x)}$. In the high-mass region, the IMF has a relatively steep slope of $x = 1.7$, while it flattens in the low-mass range ($x = 1.2$ for $0.5M_{\odot} \leq m \leq 1.0M_{\odot}$ and $x=0.3$ for $m < 0.5M_{\odot}$). The adopted IMF is normalized to $\int_{0.1}^{100.0} m\phi(m) dm = 1$.

4. Results and discussions

4.1. χ^2 -test

The observed G-dwarf metallicity distribution is treated as the tightest observational constraints on the chemical evolution models of the Galactic disk(CMG97). The metallicity of local disk stars in the sample of Hou et al (1998) extends to $[\text{Fe}/\text{H}] = -1.5$, which

is consistent with the observations of the thick disk (Majewski 1993, Nissen & Schuster 1997). However, the metal-weak tail of the thick disk is excluded from the distribution of RM96 by using a chemical criterion. Since the main aim of this work is to predict the general properties of the thick disk, we select the distribution of Hou et al (1998) as the observational constraint.

The χ^2 of the goodness-of-fit to the observed data is calculated as follows

$$\chi^2(n) = \sum_{i=1}^n \left(\frac{y_{mi} - y_{oi}}{\sigma_i} \right)^2, \quad (11)$$

where y_{mi} and y_{oi} are respectively the model-generated and observed data in i th data bin, σ_i is the error of the observed data in i th bin, and n is the total number of bins. For the metallicity distribution, Hou et al (1998) have already divided the observed data into 19 bins. The error σ_i is given by

$$\sigma_i \left(\frac{\Delta N_i}{N} \right) = \sqrt{\left(\frac{\sqrt{\Delta N_i}}{N} \right)^2 + \left(\frac{\Delta N_i}{N} \frac{1}{\sqrt{N}} \right)^2} = \sqrt{\frac{\Delta N_i}{N} \frac{1}{N} + \left(\frac{\Delta N_i}{N} \frac{1}{\sqrt{N}} \right)^2}, \quad (12)$$

where $\Delta N_i/N$ is the relative number of G-dwarfs in the i th bin and N is the total number of G-dwarfs in the corrected sample.

For comparison, we consider four different models respectively, which are closed-box, one-component, pre-thin and post-thin model. The differences among these models are the treatments of the infall rate. We perform model calculations for a broad range of free parameter combinations, if there are any, to present the best-fit to the new metallicity distribution. Using χ^2 -test, the results of best-fit to the G-dwarf metallicity distribution for these individual models are shown in table 2, which are detailedly discussed at following subsections. The characteristics of the models are shown in the first column. The resulted values of free parameters, the χ^2 and the model confidential levels for the best-fit are shown in second, third, fourth column respectively. Figure 1 presents the best-fits to the new G-dwarf metallicity distribution for closed-box model (dotted line), the one-component model (dot-dashed line), pre-thin model (long dashed line) and post-thin model (full line).

4.2. Closed-box model

The closed-box model considers the whole disk as an isolated system. Thus, $A(r) = B(r) = 0$. No free parameter exists if the closed-box model is considered. Figure 2 shows that the closed-box model predicts larger number of metal-poor stars than that of the observations. It is often called the G-dwarf problem. The fact that closed-box model does not work is also shown in table 2, where the confidential level is too low to accept the model. Several possible explanations to the G-dwarf problem have been proposed (see brief reviews in Francois et al 1990, Malinie et al 1993). Generally, a good agreement

Table 2. The results of best-fit to the new G-dwarf metallicity distribution for four different models

characteristics of the model	free parameters (best-fit)	χ^2 (best-fit)	model confidential level (best-fit)
closed-box model:			
$A(r) = 0$			
$B(r) = 0$	no	131.7	< 0.1%
one-component model:			
$A(r) = 0$			
$B(r) \neq 0$	$\tau_d = 3.8 \text{Gyr}$	20.3	30%
pre-thin model:			
$A(r) \neq 0$	$\tau_t = 1.0 \text{ Gyr}$		
$B(r) \neq 0$ ($=0$, if $t < t_{max}$)	$\tau_d = 4.0 \text{Gyr}$	14.6	70%
$t_{max} \neq 0$	$\Sigma_{thick}(r_\odot, t_g) = 14.0 M_\odot pc^{-2}$ $t_{max} = 1.0 \text{Gyr}$		
post-thin model:			
$A(r) \neq 0$ ($=0$, if $t < t_{max}$)	$\tau_t = 1.0 \text{ Gyr}$		
$B(r) \neq 0$	$\tau_d = 4.0 \text{Gyr}$	14.4	70%
$t_{max} \neq 0$	$\Sigma_{thick}(r_\odot, t_g) = 10.0 M_\odot pc^{-2}$ $t_{max} = 1.0 \text{Gyr}$		

between model predictions and observations is obtained by models that assume the disk formed by infall of primordial gas (Pilyugin & Edmunds 1996b, CMG97)

4.3. One-component model

The one-component model treats the thick and thin disk as one disk, which corresponds to the infall rate of only one Gaussian form, i.e., $A(r) = 0, B(r) \neq 0$. There is only one free parameter τ_d , i.e., the infall timescale of the whole disk in one-component model after normalization mentioned above. Figure 1 shows that, for the one-component model, the goodness-of-fit between best-fit model predictions and observations seems to be acceptable, especially for the shape of the single peak of the metallicity distribution for G dwarfs. But, the results of χ^2 -test gives that the confidential level of one-component model is some 30%, yet it can reach 70% for the two-component model (Table 2). This means one-component model is not the best, which is consistent with the observational result that the thick disk is kinematically and chemically different from the thin disk (see brief reviews in Majewski 1993). Therefore, it is necessary to treat the thick and thin disk differently, if one wants to investigate detailedly the Galactic chemical evolution.

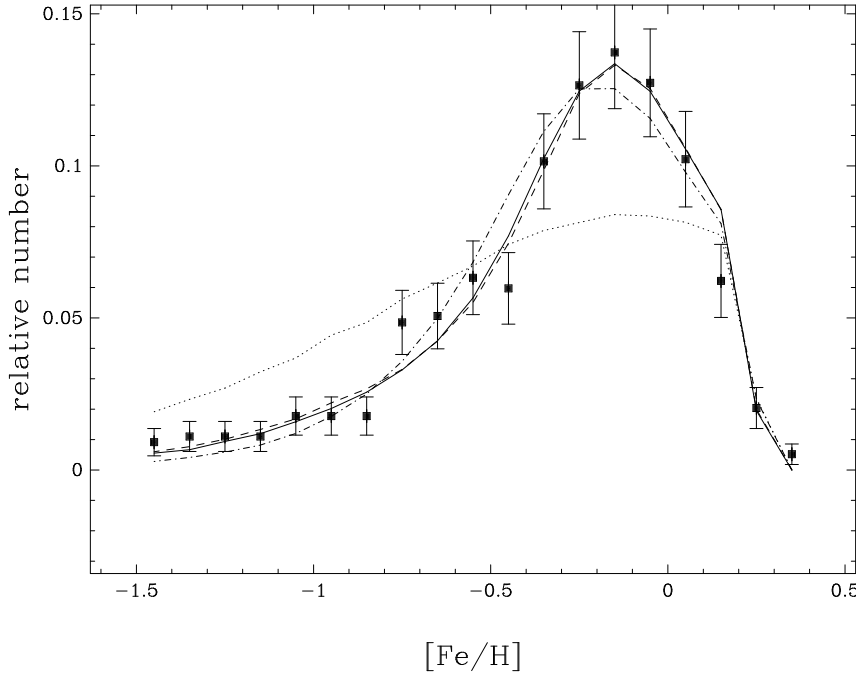


Fig. 1. The best-fits to the new G-dwarf metallicity distribution for close-box model (dotted line), the one-component model (dot-dashed line), pre-thin model (long dashed line) and post-thin model (full line). The observed data are taken from Hou et al (1998).

4.4. Two-component model

For the two-component model, both the pre-thin and post-thin model are considered. The differences between these two models are represented by different treatments of the infall rate, which are detailedly described in section 2.2. There are four free parameters in both the pre-thin and post-thin model, $\tau_t, \tau_d, t_{max}, \Sigma_{thick}(r_\odot, t_g)$. It should be emphasized that the t_{max} has different meaning in different model. Figure 1 show that, for these two models, the best-fit model predictions are in good agreement with the observations, which are confirmed by the results of quantitative tests (Table 2). From Figure 1 and Table 2, it is difficult to distinguish which model is better.

One important parameter predicted by the best-fit of our two-component model is the local surface density of thick disk at the present time. On the other hand, the density ratio of thick to thin disk are usually deduced from studies of star counts. In Table 3, we present the comparison between our model predictions and the data compiled from literatures. Since the density normalization and scale-height of the thick disk are anti-correlated when fitted simultaneously (Reid & Majeweski 1993, Majeweski 1993, Robin et al. 1996), the scale heights of the thick disk are also shown in 2th column. The previous

Table 3. Local density ratio of thick to thin disk from literatures

Authors	scale height of thick disk (pc)	space density normalization	$\Sigma_{thick}(r_\odot, t_g)$ $M_\odot pc^{-2}$
Gilmore & Reid (1983)	1450	0.020	4.85
Rose (1985)	500 \sim 1000	0.100	11.0
Friel (1987)	1000	0.050	7.85
Sandage (1987)	940	0.110	14.1
Norris (1987)	1100	0.034	6.09
Kuijken & Gilmore (1989)	1000	0.040	6.47
Reid & Majewski (1993)	1400 \sim 1600	0.020 \sim 0.025	5.67
Robin et al. (1996)	760	0.056 \pm 0.010	6.83
Ojha et al. (1996)	760	0.074 \pm 0.020	8.69
Buser et al. (1998)	1150	0.054 \pm 0.015	9.43
This paper (1999):			
pre-thin model	1000	0.113	15.0
post-thin model	1000	0.067	10.0

results for the space density ratio of thick to thin disk (the parameter D) are shown in 3th column. Taking the scale-height of thick and thin disk as $h_t = 1000$ pc and $h_d = 300$ pc respectively as usual (Majewski 1993), the local space density ratio of thick to thin disk at the present time predicted by our model can be obtained based on the following equation:

$$D \approx \frac{\Sigma_{thick}(r_\odot, t_g)}{\Sigma_{tot}(r_\odot, t_g) - \Sigma_{thick}(r_\odot, t_g)} \frac{h_d}{h_t}, \quad (13)$$

where $\Sigma_{thick}(r_\odot, t_g) = 10.0 M_\odot pc^{-2}$ and $15.0 M_\odot pc^{-2}$ for the best-fittings of the pre-thin and post-thin model, respectively. Moreover, equation (13) can also be used for deducing the $\Sigma_{thick}(r_\odot, t_g)$ with published D and h_t in literatures. The results are shown in 4th column of Table 3 with $h_d = 300$ pc and $\Sigma_{tot}(r_\odot, t_g) = 55.0 M_\odot pc^{-2}$, respectively.

From Table 3, it can be seen that the previous density normalizations of thick disk span a wide range (from 0.02 to 0.11). This is partly due to the difficulty in distinguishing the kinematical, chemical and spatial characteristics of thick disk with halo and thin disk. Moreover, comparing published star counts and color distribution in neighboring fields, star density discrepancies are sometimes larger than photometric random errors as established by authors (Ojha et al. 1996, Robin et al. 1996). But the results of more recent surveys are in good agreement within the error range (Ojha et al. 1996, Robin et al. 1996, Buser et al 1998). Table 3 shows that the value of $\Sigma_{thick}(r_\odot, t_g)$ predicted by the post-thin model are consistent with most of the previous results from literatures, while $\Sigma_{thick}(r_\odot, t_g)$ predicted by the pre-thin model is larger than the previous data

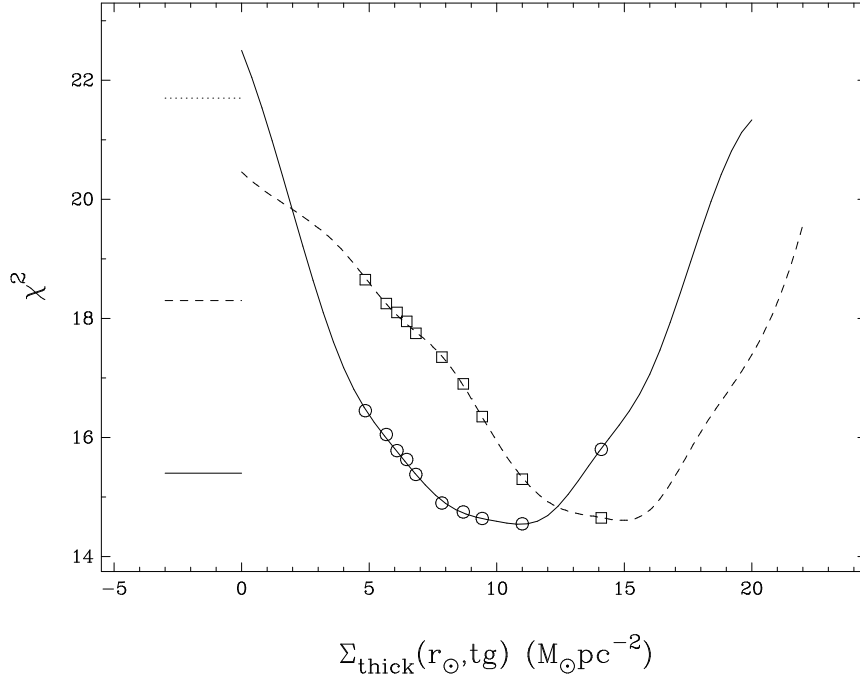


Fig. 2. The χ^2 as a function of the $\Sigma_{thick}(r_\odot, t_g)$ within reasonable range for both the pre-thin model (long dashed curve) and post-thin model (full curve) in which other free parameters are fixed as $\tau_t=1.0\text{Gyr}$, $t_{max}=1.0\text{Gyr}$ and $\tau_d=4.0\text{Gyr}$. Three short horizontal lines indicate the model confidential level of 30% (dotted line), 50% (long dashed line) and 70% (full line), respectively. The points indicate the different results of χ^2 if the value of $\Sigma_{thick}(r_\odot, t_g)$ from ten literatures (Table 3) are adopted for both the pre-thin model (open squares) and post-thin model (open circles), respectively.

from studies of star counts. To illustrate this quantitatively, Figure 2 shows the χ^2 as a function of the $\Sigma_{thick}(r_\odot, t_g)$ within reasonable range for both the pre-thin model (long dashed curve) and post-thin model (full curve) in which other free parameters are fixed as $\tau_t=1.0\text{Gyr}$, $t_{max}=1.0\text{Gyr}$ and $\tau_d=4.0\text{Gyr}$. It is shown that the value of χ^2 is very sensitive to $\Sigma_{thick}(r_\odot, t_g)$. This suggests that the thick disk has great influence on the Galactic chemical evolution. In figure 2, three short horizontal lines indicate the model confidential level of 30% (dotted line), 50% (long dashed line) and 70% (full line), respectively. The points in Figure 2 indicate the different results of χ^2 if the value of $\Sigma_{thick}(r_\odot, t_g)$ from ten literatures (Table 3) are adopted for both the pre-thin model (open squares) and post-thin model (open circles), respectively.

Figure 2 shows that, for the post-thin model, five points have model confidential level larger than 70%, while only two points have confidential level larger than 70% for the pre-thin model. This suggests that the post-thin model be better than pre-thin model. Other

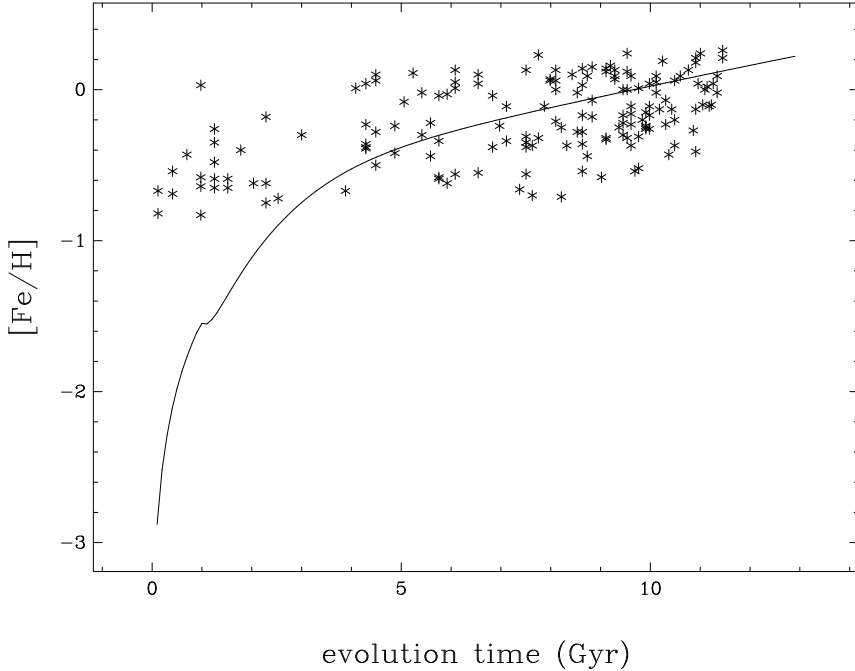


Fig. 3. Temporal evolution of [Fe/H] predicted by the best-fit model (full line) for the solar vicinity. The observed data (asterisks) are from Edvardsson et al (1993).

evidences tended to favour the post-thin scenario for the formation of thick disk comes from the following facts. First, the thick disk is kinematically distinct from the thin disk and it shows no kinematic gradients (Ojha et al 1994 a,b). Second, Gilmore et al (1995) studied metallicity distribution of thick disk stars up to about 3kpc from the Galactic plane. They found that thick disk stars show no vertical abundance gradient. This argues against dissipational setting as the formation process of the thick disk (Freeman 1996).

4.5. Discussions

Based on the above discussions, we treat the post-thin model with $\tau_t=1.0$ Gyr, $t_{max}=1.0\text{Gyr}$, $\tau_d=4.0$ Gyr and $\Sigma_{thick}(r_\odot, t_g)=10.0M_\odot\text{pc}^{-2}$ as the best-fit model.

Figure 3 presents the comparison between our best-fit model predictions for the AMR and the observations. The full line is our model predictions and the points are observational data taken from Edvardsson et al (1993). Figure 3 shows that, at the beginning of the formation of the thick disk ($t = t_{max} = 1.0\text{Gyr}$), the iron abundance of ISM decreases a little due to the increasing infall rate of the primordial gas. After that phase, the model predicts that the metallicity increases smoothly with time. The overall tendency for this relation is consistent with the mean observations, but the present model can not

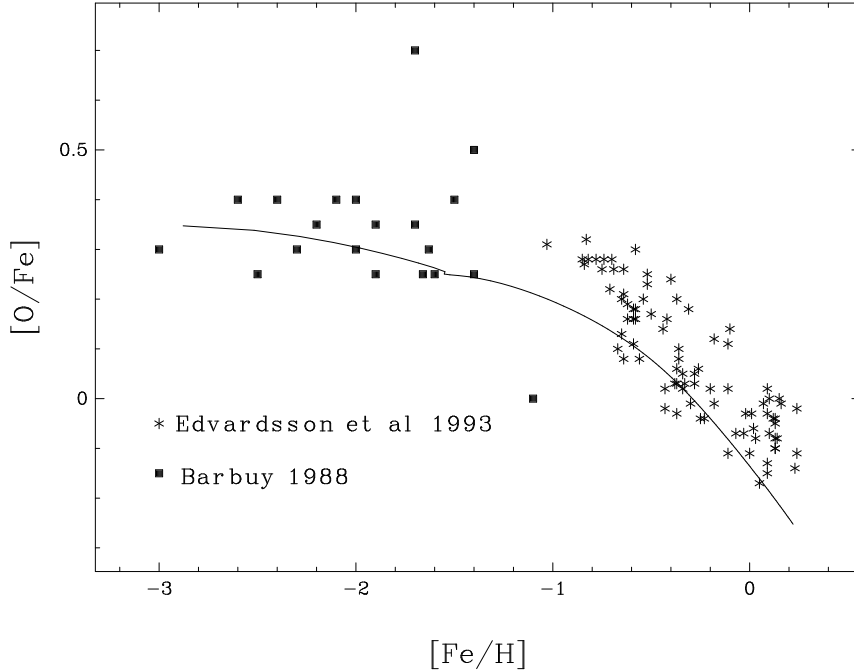


Fig. 4. Predicted behavior of $[O/Fe]$ vs. $[Fe/H]$ for the best fit model (full line). The observed data are from Edvardsson et al (1993) (asterisks) and Barbuy (1988) (full squares).

reproduce the large observed scatters. Nordstrom et al. (1997) discussed in detail the main hypotheses for the origin of this scatter, such as star formation in an inhomogeneous gaseous medium, orbital diffusion in homogeneous galaxy and mergers or accretion events. However, a physical mechanism that reproduces the observed scatter in the AMR without violating other observational constraints has not yet been identified.

Figure 4 compares the predicted behaviors of $[O/Fe]$ vs. $[Fe/H]$ for the best-fit model (full line) with the observations. The observed data are taken from Edvardsson et al (1993) (asterisks) and Barbuy (1988) (full squares). Our model predicts that there is a small loop at $[Fe/H] = -1.6$. The similar behavior is predicted in the best-fit model of CMG97. Figure 4 shows that our model prediction is in good agreement with the observations. This suggests that the relative stellar yield for oxygen and iron we adopted here be reasonable.

Contrary to the case of the solar neighbourhood, the available observations for the Milky Way disk offer information mainly about its current status, not its past history. Therefore, there is much more freedom in constructing a model. Up to now, chemical evolution models of the Galactic disk consider the disk as a system of independent rings. This oversimplification generally ignores the possibility of radial inflows produced in

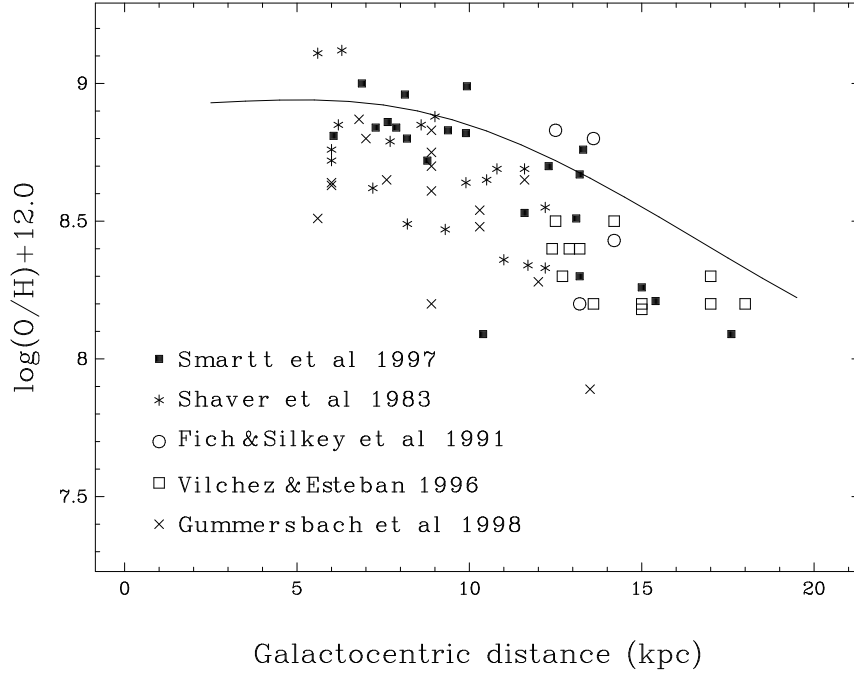


Fig. 5. Radial distribution of the oxygen abundance at the present time predicted by the best-fit model (full line). The observed data of HII regions are from Shaver et al (1983) (asterisks), Fich & Silkey (1991) (open circles) and Vilchez & Esteban (1996) (open squares). The observations of early B-type main-squence stars are taken from Smartt et al (1997) (full squares) and Gummersbach et al (1998) (crosses).

gaseous disks, e.g. by viscosity or by the infall of gas with a specific angular momentum different from that of the underlying disk (Prantzos & Silk 1998). Fortunately, a radial variation of the infall time-scale may play a similar role. In our best-fit model, the infall timescale of the thin disk τ_d is assumed to be radially dependent, taking an lower values in the inner disk ($\tau_d=2$ Gyr at $r=2$ kpc) and larger ones in the outer disk ($\tau_d=4$ Gyr at $r=8.5$ kpc).

In Figure 5, we compare the predicted radial distribution of oxygen abundances by our best-fit model (full line) with the observations. The observed data of HII regions are from Shaver et al (1983) (asterisks), Fich & Silkey (1991) (open circles) and Vilchez & Esteban (1996) (open squares). The observations of early B-type main-squence stars are taken from Smartt et al (1997) (full squares) and Gummersbach et al (1998) (crosses). It shows that model predictions of oxygen abundances are larger than most of the observations. Moreover, our model predicts that the abundance gradient in inner region (-0.01 dex/kpc for $r \leq 8.5$ kpc) is steeper than that in outer region (-0.07 dex/kpc for $r \geq 8.5$ kpc). This seems to be contradictory to the observations of HII region, which suggests a flatter

oxygen abundance gradients in outer region. This disagreement was also obtained by most of chemical evolution models for the Galactic disk (see brief reviews in Tosi 1996). This is probably due to the simplicities of the present models. Samland et al. (1997) developed a chemi-dynamical evolution model for the Galactic disk and presented better fit for the observed variations of oxygen abundance across the whole disk. Therefore, this disagreement probably could be solved if one considers the influence of dynamical evolution on the chemical evolution and the effect of gas heating on star formation rate.

Figure 6 presents the comparison between the predictions of our best-fit model for the radial profile of the present SFR (full line) and the observations. Observed data are normalized to SFR in the solar neighborhood. Data are based on several tracers of star formation: Lyman continuum photons from HII regions (full squares, from Gusten & Merger 1983); pulsars (open circles: from Lyne et al 1985); and supernova remnants (crosses: from Guibert et al 1978). The good agreement between our model prediction and the observations indicates that our model predicts reasonable star formation history for the Galactic disk.

Finally, in Figure 7, we present the comparison for the radial distribution of the present gas surface density between our best-fit model predictions (full line) and the observations (dashed lines). Two dashed lines are reproduced from Prantzos & Aubert (1995). The lower dashed line is the sum of atomic and molecular hydrogen given in Dame (1993), corrected for the contribution of 30% helium. The upper one is obtained by adopting the gas surface density in the solar neighbourhood as $16 M_{\odot} pc^2$ and scaling the curve of Dame (1993) accordingly (Prantzos & Aubert 1995). Given the uncertainties in the observational data, the model is also in good agreement with the observed profile.

5. Conclusions

In this work, we introduce a two-component models for the chemical evolution of the Galactic disk, which assumes that the formation of the thick and thin disks occur in two main accretion episodes. The infall rate is assumed to be Gaussian. Both the pre-thin and post-thin scenarios for the formation of the Galactic disk are considered. The local surface density of the thick disk at the present time is chosen to be one of the free parameters. Following Prantzos & Silk (1998), we also assume that the SFR is not only proportional to n power of gas surface density, but directly correlates with the Galactocentric distance. Comparing model predictions with the new metallicity distribution in the solar neighbourhood (Hou et al 1998), we use the χ^2 -test to derive best-fittings and compare the reasonableness of four different models, which are closed-box, one-component, pre-thin and post-thin models. Moreover, comparisons between the predictions of our

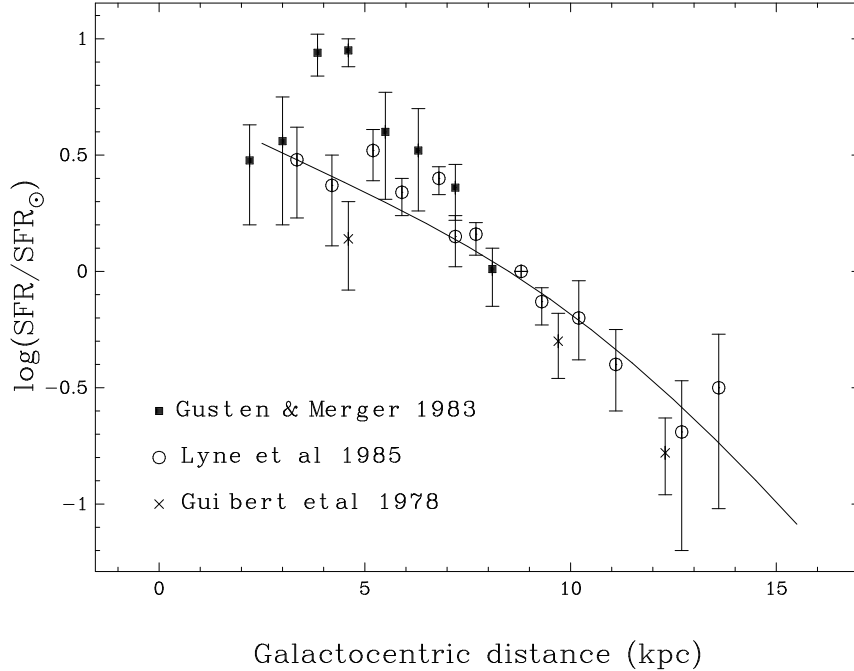


Fig. 6. Profile of present star formation rate (SFR) in the galactic disk. Full line is the predictions of the best-fit model. Observed data are normalized to SFR in the solar neighborhood. Data are based on several tracers of star formation: Lyman continuum photons from HII regions (full squares, from Gusten & Merger 1983); pulsars (open circles: from Lyne et al 1985); and supernova remnants (crosses: from Guibert et al 1978).

best-fit model and the main observational constraints are presented. The main results can be summarized as follows.

1. Our results suggests that the post-thin model for the formation of the Galactic disk should be preferred. This is consistent with the observational evidences that the thick disk is chemically and kinematically distinct from the thin disk and it shows no vertical abundance gradient.
2. The goodness-of-fit for model predictions about metallicity distribution to the observations, χ^2 , is very sensitive to the local surface density of the thick disk at the present time. This suggests that it is necessary to treat the thick and thin disks differently if one want to investigate detailedly the Galactic chemical evolution.
3. The post-thin model predicts $\Sigma_{thick}(r_{\odot}, t_g) = 10.0 M_{\odot} pc^{-2}$. The resulted space density ratio of thick to thin disk is consistent with the previous data from recent studies of

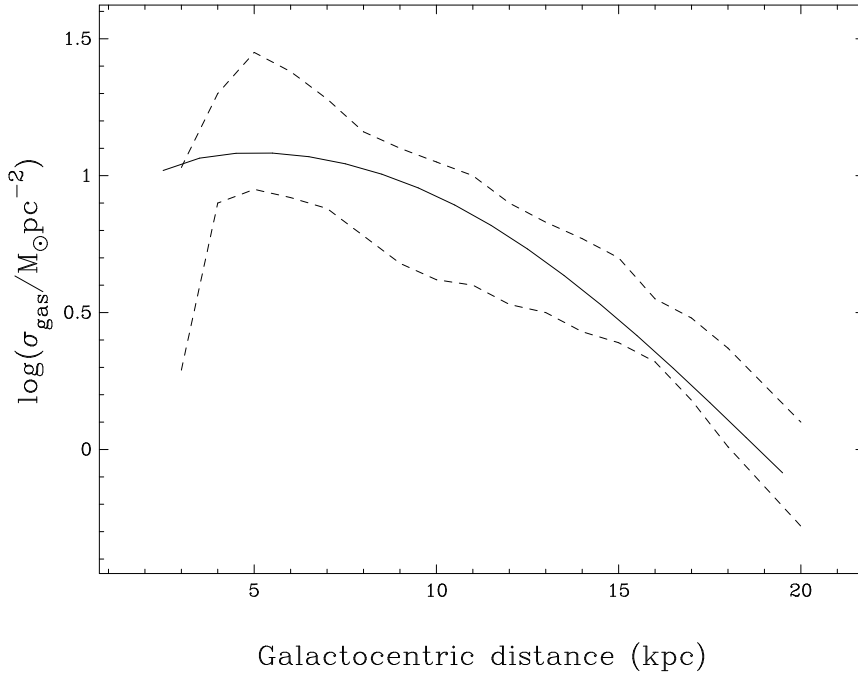


Fig. 7. Radial distribution of the present gas surface density predicted by the best-fit model (full line). The lower dashed line is the sum of atomic and molecular hydrogen given in Dame (1993), corrected for the contribution of 30% helium. The upper one is obtained by adopting the gas surface density in the solar neighbourhood as $16 M_{\odot} pc^2$ and scaling the curve of Dame (1993) accordingly (Prantzos & Aubert 1995).

star counts. However, the pre-thin model predicts a larger value of the local thick disk density.

4. The predictions of our best-fit model are in good agreement not only with the observed data in the solar neighborhood, but also with the main observational features of the Galactic disk. However, contrary to the observations in HII regions, our model predicts the oxygen abundance gradient in outer region is steeper than that in inner region.

Acknowledgements. The authors wish to thank Prof. Peng Qiuhe of Nanjing University for helpful discussions. This research was supported in part by a grant from the National Natural Science Foundation of China and in part by the grant from Young Lab of Shanghai Observatory.

References

Afflerbach A., Churchwell E., Acord J.M. et. al. 1996, ApJS 106, 423
 Allen C., Carigi L. & Peimbert M., 1998, ApJ 494, 247
 Barbuy B., 1988, A&A 191, 121
 Buser R. & Kaeser U., 1985, A&A 145, 1

Buser R., Rong J.X. & Karaali S., 1998, A&A 331, 934

Carigi L., 1996, Rev.Mex.A.A. 32, 179

Carlberg R.G., Dawson P.C., Hsu, T. & VandenBerge D.A., 1985, ApJ 294, 674

Chiappini C., Matteucci F. & Gratton R., 1997, ApJ 477, 765 (CMG97)

Dame T.M., in "Back to the Galaxy", eds. S.Holt and F. Verter (AIP), p.267

Edvardsson B., Andersen J., Gustafsson B. et al., 1993, A&A 275, 101

Eggen O.J., Lynden-Bell D. & Sandage A.R., 1962, ApJ 136, 748

Ferrini F., Molla M., Pardi C. & Diaz A.I., 1994, ApJ 427, 745

Fich M. & Silkey M., 1991, ApJ 366, 107

Francois P., Vangioni-Flam E. & Audoze J., 1990, ApJ 361, 487

Freemann K.C., 1996, in IAU Symposium 171, New Light on Galaxy Evolution, eds. R. Bender & R.L. Davies, p.1

Friel E.D., 1987, AJ 93, 1388

Gilmore G.F. & Reid I.N., 1983, MNRAS 202, 1025

Gilmore G.F., Reid I.N. & Hewett P.C., 1985, MNRAS 213, 257

Gilmore G.F., Wyse R. & Jones B., 1995, AJ 109, 1095

Giovagnoli A. & Tosi M., 1995, MNRAS 273, 499

Guibert J., Lequeux J. & Viallefond F., 1978, A&A 68, 1

Gliese W., Jahreiss H., Third Catalogue of Nearby Stars. Astron. Rechen-Inst. Heidelberg

Gummersbach C.A., Kaufer A., Schafer D.R., Szeifert T. & Wolf B., 1998, A&A 338, 881

Gusten R. & Mezger M., 1983, Vistas Astr. 26, 159

Hauck B. & Mermilliod M., 1990, A&AS 86, 107

Hou J.L., Chang R.X. & Fu C.Q., 1998, Annals of Shanghai Observatory Academia Sinica, No. 19, 96

Kauffmann G., White S.D.M. & Guiderdoni B., 1993, MNRAS 264, 201

Kauffmann G., Colberg J.M., Diaferic A. & White S.D.M., 1998, MNRAS in press (astro-ph 9805283)

Kennicutt R.C. Jr., 1989, ApJ 344, 685

Kennicutt R., 1998, ApJ 498, 541

Kent S., 1992, ApJ 387, 181

Kroupa P., Tout C. & Gilmore G., 1993, MNRAS 262, 545

Kuijken K. & Gilmore G., 1989, MNRAS 239, 605

Lacey C.G. & Fall M., 1985, ApJ 290, 154

Larson R.B., 1974, MNRAS 166, 585

Larson R.B., 1976, MNRAS 176, 31

Lyne A., Manchester R. & Taylor J., 1985, MNRAS 213, 613

Majewski S.K., 1993, ARA&A 31, 575

Malinie G., Hartmann D.H., Clayton D.D. & Mathews G.J., 1993, ApJ 413, 633

Matteucci F. & Francois P., 1989, MNRAS 239, 885

Matteucci F. & Greggio, L. 1986, A&A 154, 279

Mo H.J., Mao S. & White S.D.M., 1998, preprint (astro-ph 9807341)

Nissen P.E. & Schuster W.J., 1997, A&a 326, 751

Nordstrom B., Olsen E.H. & Andersen J., 1997, in ASP Conf. Series, 112, The History of the Milky Way, ed. A. Burkert, D.H. Hartmann & S.R. Majewski, p. 144

Norris J.E., 1987, ApJ 314, L39

Ojha D.K., Bienayme O., Robin A.C. & Mohan V., 1994a, A&A 284, 810

Ojha D.K., Bienayme O., Robin A.C. & Mohan V., 1994b, A&A 290, 771

Ojha D.K., Bienayme O., Robin A.C., Creze M. & Mohan V., 1996, A&A 311, 456

Olsen E.H., 1993, A&AS 102, 89

Pagel B.E.J., 1997, Nucleosynthesis and Galactic Chemical Evolution (Cambridge: Cambridge Univ. Press)

Pagel B.E.J. & Patchett B.E., 1975, MNRAS 172, 13

Pagel B.E.J., 1989, in Evolutionary Phenomena in Galaxies, ed. J. Beckman & B.E.J. Pagel (Cambridge: Cambridge Univ. Press), p. 201

Pilyugin L.S. & Edmunds M.G., 1996a, A&A 313, 792

Pilyugin L.S. & Edmunds M.G., 1996b, A&A 313, 783

Prantzos N. & Aubert O., 1995, A&A, 302, 69

Prantzos N. & Silk J., 1998, ApJ 507, 229

Primack J.R., Bullock J.S., Somerville R.s. & MacMinn D., 1999, preprint (astro-ph 9812141)

Quinn P.J., Hernquist L. & Fullager D.P., 1993, ApJ 403, 74

Rana N.C., 1991, ARA&A 29, 129

Reid N. & Majewski S.R., 1993, ApJ 409, 635

Robin A.C., Haywood M., Creze M., Ojha D.K. & Bienayme O., 1996, A&A 305, 125

Rose J.A., 1985, AJ 90, 787

Rocha-Pinto H.J. & Maciel W.J., 1996, MNRAS 279, 447

Sackett P.D., 1997, ApJ 483, 103

Samland M., Hensler G. & Theis C.H., 1997, ApJ 476, 544

Sandage A., 1990, J.R.Astron.Soc.Con. 84, 70

Sandage A., 1987, AJ 93, 610

Scoville N. & Sanders D., 1987, in "Interstellar Processes", Eds. H. Thronson & D. Hollenbach (Kluwer) P. 21

Shaver P.A., McGee R.X., Newton L.M., Danks A.C. & Pottasch S.R., 1983, MNRAS 204, 53

Smartt S.J. & Rolleston W.R.J., 1997, ApJ 481, L47

Sommer-Larsen J., 1991, MNRAS 249, 368

Somerville R.S. & Primack J.R., 1998, MNRAS in press (astro-ph 9802268)

Thon R., & Meusinger H., 1998, A&A 338, 413

Timmes, T.X., Woosley, S.E. & Weaver, T.A., 1995, ApJS 98, 617

Tinsley B., 1980, Fundam. Cosmic Phys. 5, 287

Tosi M., 1996, in ASP Conf. Proc. 98, From Stars to Galaxies, ed. C. Leitherer, U. Fritze-von Alvensleben & J. Huchra (San Francisco: ASP), p. 299

Twarog B.A., 1980, ApJ 242, 242

van den Hoek L.B. & Groenewegen M.A.T., 1997, A&AS 123, 305

Vilchez J.M. & Esteban C., 1996, MNRAS 280, 720

Wang B. & Silk J., 1994, ApJ 427, 759

Wechsler R.H., Gross M.A.K., Primack J.R., et al 1998, preprint (astro-ph 9712141)

Weideman V., 1984, A&A 134, L1

White S.D.M. & Frenck C.S., 1991, ApJ 379, 52

White S.D.M. & Rees M.J., 1978, MNRAS 183, 341

Woosley S.E. & Weaver T.A., 1995, ApJS 101, 181

Woosley S.E., 1997, ApJ 476, 801